Mechanics of lithographically defined break junctions

S. A. G. Vrouwe,[1] E. van der Giessen,[1] S. J. van der Molen,[2] D. Dulic,[2] M. L. Trouwborst,[2] and B. J. van Wees[2]

[1]*Micromechanics of Materials, Materials Science Centre, Nijenborgh 4, 9747 AG Groningen, The Netherlands*
[2]*Physics of Nanodevices, Materials Science Centre, Nijenborgh 4, 9747 AG Groningen, The Netherlands*

We investigate the mechanics of lithographically defined mechanically controllable break junctions, both theoretically and experimentally. It is shown that the relationship between controlled deflection and junction opening depends on the details of the break junction geometry. As a result the generally used formula for the "attenuation factor" r needs to be corrected by a factor ζ. For typical break junction geometries, we obtain $2 \lesssim \zeta \lesssim 4$.

I. INTRODUCTION

The mechanically controllable break junction (MCBJ) technique is a very elegant way to control the spacing between two metallic electrodes with subatomic ($< 10^{-10}$ m) resolution.[1–3] The concept of a "break junction" was first introduced in 1985 by Moreland and Ekin[1] for the study of the tunneling characteristics of superconductors. Since then the method has been modified and developed further by Muller *et al.*[2] and Van Ruitenbeek *et al.*[3] for the study of electronic transport processes in atomic-size metallic point contacts and wires. Although the fabrication of particular devices may differ, the idea behind the MCBJ is very simple. A thin metal wire is attached on top of a bending beam which has a certain degree of flexibility. By applying a force on the back side of the substrate, the beam is bent and consequently the wire is extended and finally broken, most likely along grain boundaries at the notch. This creates two electrodes with fresh surfaces. Subsequently, it is possible to control the distance between the newly formed electrodes by moving the pushing rod. Moreover, due to the tiny value of the "attenuation factor" r—defined as the ratio of the elongation in the wire direction Δd, and the translation of the pushing rod u_2 (see Fig. 1)—this can be done with an impressive precision, even better than scanning tunneling microscopy.[4] Another important feature of the MCBJ is that the breaking process creates rather sharp (i.e., low radius) electrode tips, so that conduction is dominated by one or a few atoms only.[4] As a result of their good tunability and sharp electrodes, break junctions are excellent devices for transport measurements, even on single molecules.[5–9]

A general procedure to capture molecules in a gold break junction is as follows. First, the junction is broken. Second, the electrode distance is set to a value somewhat larger than the length of the molecules of interest. This can only be done accurately if the attenuation ratio r is precisely known. Third, a droplet of solution containing molecules with two thiol end groups (a simple example being benzene-1,4-dithiol[5]) is introduced onto the break junction with a microsyringe. As soon as the molecules reach the gold, the protective acetyl groups split off and an incomplete self-assembled monolayer is formed at each of the two electrodes.[10] Finally, the inter-electrode spacing is decreased slowly, until one (or a few)

molecule(s) bridge the gap between the two gold contacts. The latter procedure is usually done while applying a voltage (~ 0.5 V), resulting in a strong field ($\sim$ V/nm) that aligns the molecules.[8,9]

To obtain a high success rate in capturing molecules, it is essential to know the value of the attenuation factor r accurately, in order to tune the distance between the electrodes at a value close to the molecular length. Based on geometrical considerations of bending, a simple formula for r can be derived for an elastically homogeneous system subject to a central deflection u_2.[3] Clearly, r depends on the break junction geometry, specifically on the distance between the countersupports, L, the substrate thickness t, and the bridge length U (for details, see Fig. 1):

$$r = \Delta d / u_2 = 6 t U / L^2. \qquad (1)$$

Though widely used, formula (1) ignores the fact that lithographically defined break junctions, as shown in Fig. 1, have inhomogeneous elastic properties and somewhat geometrically complex structures. In this contribution, we investigate the applicability of Eq. (1) to MCBJ's having both a soft polyimide and a lithographically defined gold bridge on top of the substrate. After introducing the exact break junction geometry first, we calculate r using three-dimensional finite element analysis. From this we find that Eq. (1) should be corrected by a significant factor ζ, which is roughly between 2 and 4 for typical MCBJ structures. This result is confirmed by calibration measurements on lithographically defined MCBJ's.

II. BREAK JUNCTION GEOMETRY

We focus our attention on lithographically defined MCBJ's.[3,4] These break junctions are similar to the ones we use to measure single-molecular transport.[9] To produce these devices, we start with a polished phosphor bronze substrate, which is chosen because it is ductile. The planar dimensions are 22×10 mm^2, and the substrate thickness is $t = 0.42$ mm. We then spin coat a layer of polyimide on top of the conductive substrate, which provides electrical insulation of the junction. The typical thickness of the layer is ≈ 1 μm. On top of the polyimide we pattern the device by conventional electron beam lithography. Prior to the deposition of gold
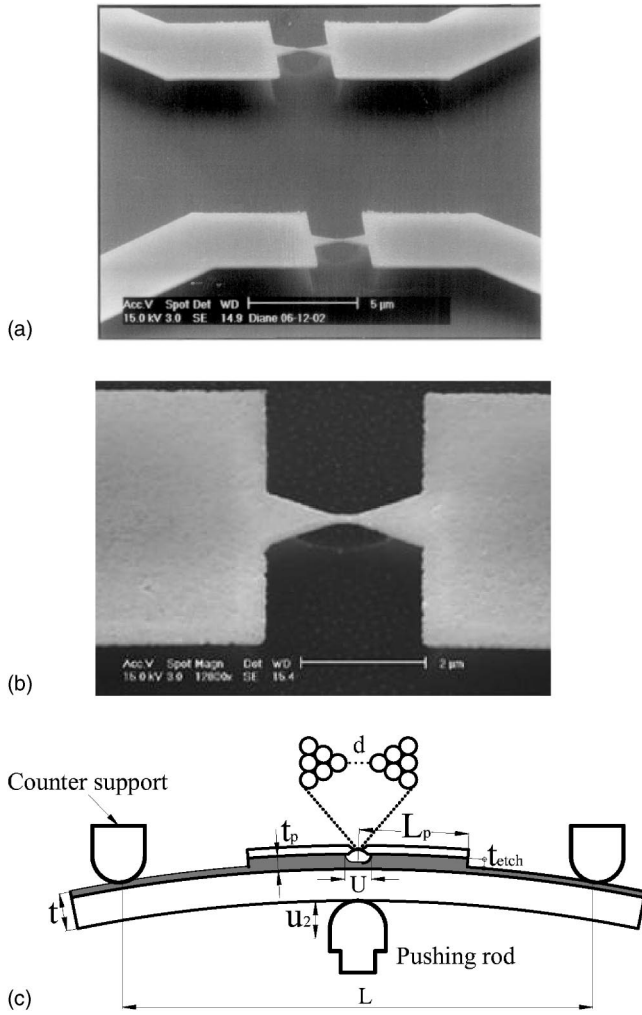
(a)

(b)

(c)

FIG. 1. (a) Scanning electron micrograph of the gold structure defined on the polyimide layer, displaying two free-hanging bridges and their connecting leads. We define L_p as the distance from the middle of the gold bridge to the kink in the lead. The scale bar length is 5 μm. (b) Scanning electron micrograph of the free-hanging bridge. The scale bar length is 2 μm. (c) Schematic layout of the sample in a three-point bending setup. The elongation of the bridge can be tuned by the pushing rod directly below it. In (c) we also define parameters used. Note the difference between bridge length U (and its increase ΔU) and the interelectrode distance d (and its increase Δd). The original polyimide thickness is denoted by t_p, whereas the thickness of the etched layer equals $t_p - t_{etch}$.

(115 nm on top of a 5 nm titanium adhesion layer), we roughen the surface of the polyimide with Kaufmann (Ar) etching for better adhesion. After gold deposition, the polyimide directly below the bridge is etched away, down to a depth t_{etch}, by reactive ion etching. This leaves behind a free-standing gold bridge. A scanning electron micrograph of the resulting structure is shown in Fig. 1(a), displaying two break junctions and their connecting leads. The leads consist of two parts. One part, connecting directly to the central structure, has a length of 5 μm; the other part makes an angle of 45° with the first part and leads to the bonding wires. Figure 1(b) presents a higher-magnification micrograph focusing on the free-standing gold bridge. The suspended length of the bridge is $U = 2.4$ μm, and the width is 100 nm at the narrowest point. We break the bridge by bending it with a three-point bending mechanism. The central part of this construction is a pushing rod whose position u_2 can be manually controlled with micrometer precision [see Fig. 1(c)]. Two countersupports at distance $L = 18.8$ mm complete the bending setup. For our break junction geometry, Eq. (1) implies that $r = 6tU/L^2 = 1.7 \times 10^{-5}$. As a consequence, a 1 μm displacement u_2 should result in a 170 pm change in interelectrode distance. This illustrates the great potential of break junctions for nanoelectronics.

III. THEORY

A. Bending of the substrate

Equation (1) is derived from standard elastic beam theory in solid mechanics.[11] The situation sketched in Fig. 1(c) is modeled as a slender beam (i.e., $L \gg t$) in two-dimensional $x_1 - x_2$ space with properties of the substrate material; see Fig. 2(a). The effect on the bending properties of the polyimide layer and the break junction itself are ignored since their thickness is several orders of magnitude smaller than t. Another essential assumption is that deformations remain so small that deviations from the original geometry can be neglected (in the range of medium deformations where this assumption starts to break down, the relative error is on the order of the strain).

The load P needed to deflect the center of the beam by a displacement u_2 in the x_2 direction induces a bending moment $M(x)$,

$$M = \frac{1}{2}P\left(\frac{1}{2}L - x_1\right). \tag{2}$$

At each position x_1 this moment gives rise to a linear normal stress distribution across the cross section relative to the neutral axis $x_2 = 0$; Fig. 2(b). Since all other in-plane stress components (approximately) vanish, linear elastic material behavior described by Hooke's law reduces to

$$\sigma_{11}(x_2) = E\varepsilon_{11}(x_2)$$

for the normal stress (σ_{11}) and associated strain (ε_{11}), with E being Young's modulus (possibly modified to account for constraint effects when the specimen is wide compared to its length). As a consequence, the bending moment can be expressed as

$$M(x_1) = \frac{EI\varepsilon_{max}(x_1)}{t/2} \tag{3}$$

where ε_{max} is the strain at the outer fiber of the beam, $\varepsilon_{max} = \varepsilon(x_2 = t/2)$. Furthermore, $I = wt^3/12$ is the plane moment of inertia, with w the width of the beam. Bending gives rise to curvature $d^2u_2/dx_1^2 = -M/EI$, integration of which along x_1 leads to the deflection

$$u_2 = \frac{PL^3}{48EI}$$

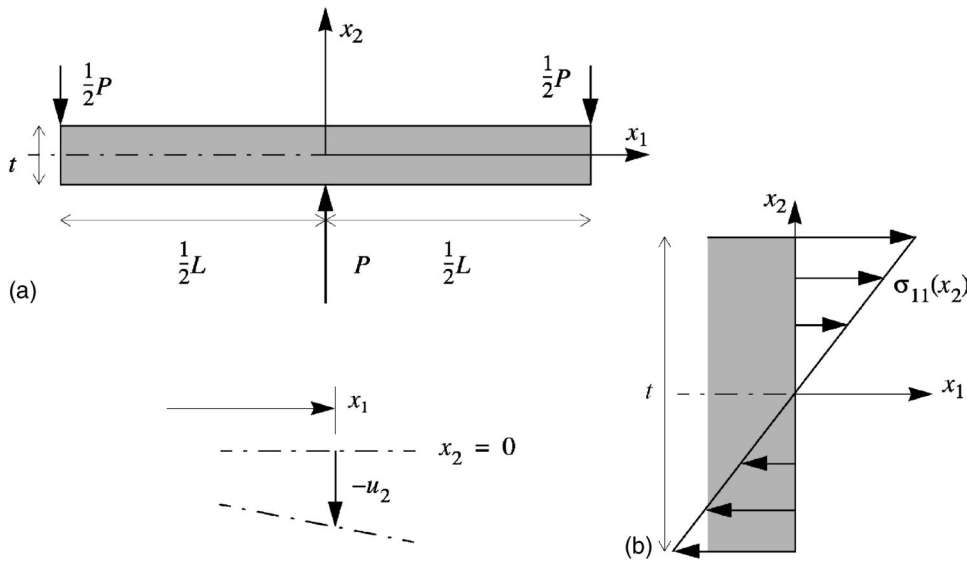of the center of the beam, at $x_1 = 0$, when the end points $x_1 = \pm L/2$ are fixed.

FIG. 2. (a) The strip is modeled as a slender beam of length L and thickness t subject to three-point bending with a central force P, which bends it relative to the neutral axis $x_2=0$ by a deflection $u_2(x)$. (b) Pure bending induces a linear variation of tensile stress σ_{11} over the cross section.

Points in the beam not only deflect in the x_2 direction, but also move in the x_1 direction. Using the strain definition $\varepsilon_{11}=\partial u_1/\partial x_1$ and the expressions (2) and (3), we can write the displacement along the top of the surface as

$$u_1(x_1) = \frac{tPL^2}{8EI}\left(\frac{x_1}{L}\right)\left[1-\left(\frac{x_1}{L}\right)\right] = \frac{6tu_2}{L}\left(\frac{x_1}{L}\right)\left[1-\left(\frac{x_1}{L}\right)\right]. \tag{4}$$

The displacement u_1 of a point $x_1=U/2$ is then, to first order, given by

$$u_1 = \Delta U/2 = \frac{6tu_2 U/2}{L^2} \tag{5}$$

when $U\ll L$. Multiplication by a factor of 2, to incorporate the other half of the bridge for $x_1<0$, recovers Eq. (1) if Δd is identified with ΔU.

It is noted that the analysis applies only as long as the material is linear elastic. As discussed previously, the first stage in applying a break junction is to break the junction by forcing the central deflection. During this process, the strip may start to deform plastically (which is observed from the fact that the strip does not return to its original flat shape upon release) and Eq. (5) does not apply. However, the bro-

ken state is the point of reference for the actual measurements, from which one makes use of the fact that unloading from a plastically deformed state is elastic. Equation (5) is then used for the small deflection excursions from that state during resistance measurements. The maximum allowable deflection before plastic deformation happens again (at a yield stress σ_y) is $u_2=\frac{1}{6}(\sigma_y/E)L^2/t$.[11]

B. Bridge deformation

It is Van Ruitenbeek *et al.*'s assumption[3] that the displacement of the tip of the junction, $\Delta d/2$, is the same as that of the point $x_1=U/2$ on the substrate surface, i.e., equal to $\Delta U/2=u_1(x_1=U/2)$. This, in fact, assumes that the transduction through the polyimide layer takes place in a rigid manner. To investigate this in detail a three-dimensional model of the near-junction region is considered, as illustrated in Fig. 3. Only one half of the junction is considered, $x>0$,[12] with a rectangular Au lead on top of a dam of height t_p-t_{etch} that is left after etching the polyimide film of original thickness t_p. Underetching is assumed to occur so as to leave a 60° ramp. The polyimide film is perfectly bonded to the substrate and follows the displacements as given by Eq. (4). Note that the nonlinear part of Eq. (4) can be safely neglected at this scale
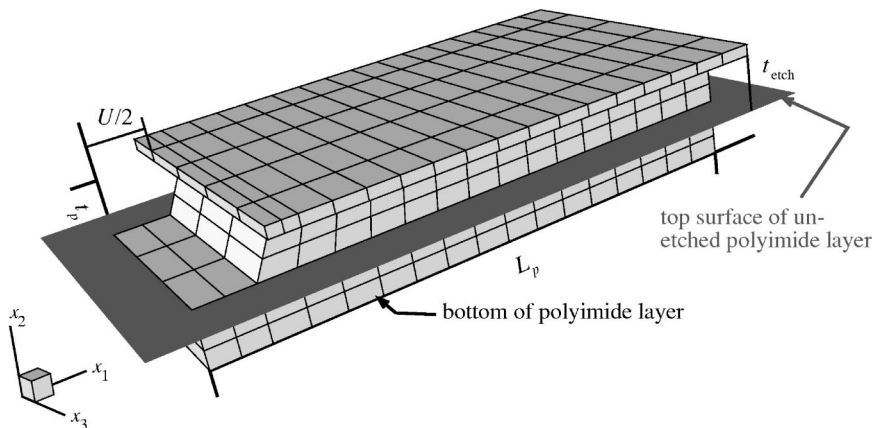

FIG. 3. Schematic of the junction model as analyzed by three-dimensional finite element analysis. The shaded surface indicates the depth to which the polyimide layer has been etched away, t_{etch}, leaving a layer of thickness t_p-t_{etch}.

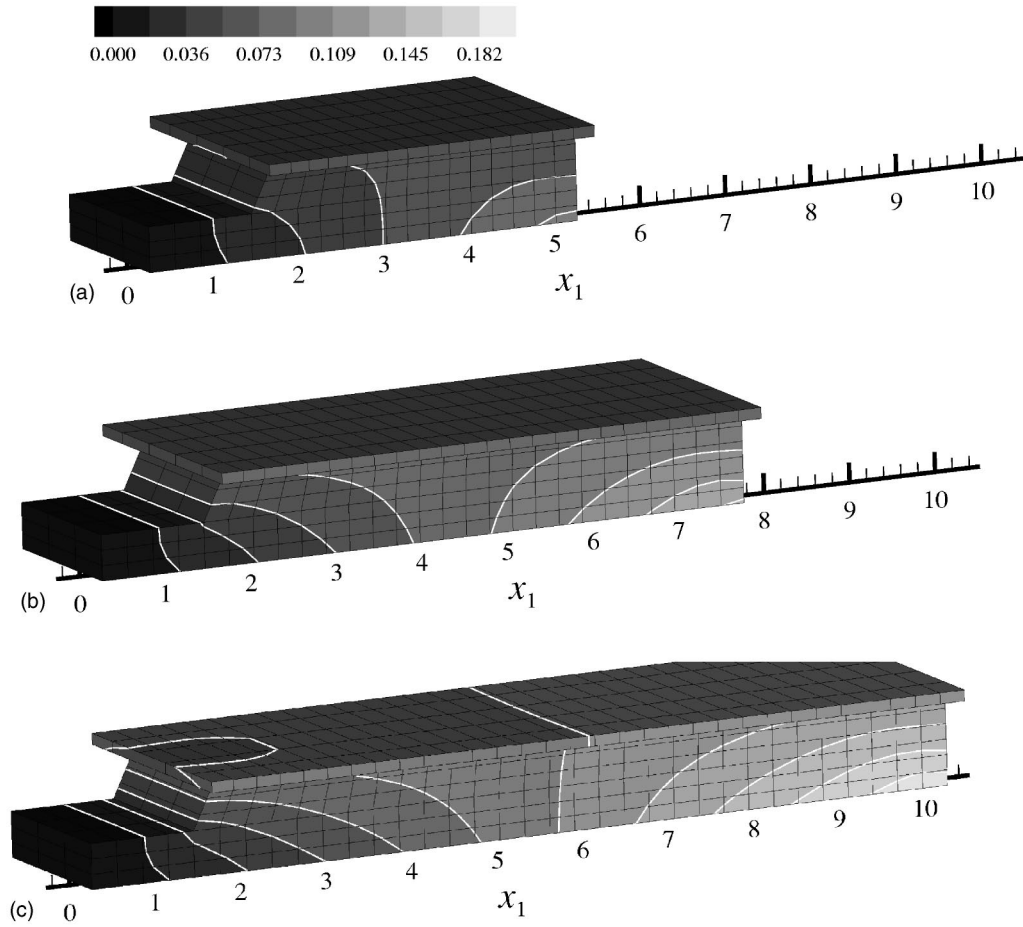FIG. 4. Contours of equal displacement u_1 in x_1 direction (in μm) for break junctions of length $L_p=5$ (a), 7.5 (b), and 10 μm (c) and with an etch depth of $t_{etch}=0.5$ μm. The substrate displacements are prescribed according to Eq. (1) with $6tu_2/L^2=0.02$.

of observation. The unetched part of the polyimide layer is treated as being infinitely wide in the x_3 direction, as is the substrate, and is therefore constrained to have zero u_3 displacements. The tip of the bridge itself is not modeled since this will move in a rigid fashion. Thus, we take the calculated displacement of the front of the Au lead at $x_1=U/2$ as half the tip displacement $\Delta d/2$.

The bridge half length $U/2$ is taken to be 1.2 μm and the etch depth t_{etch} is varied between $t_{etch}=t_p=0.75$ μm and a very small value 0.05 μm. The width of the Au lead is taken to be 3 μm and it is resting on top of a 2-μm-wide polyimide dam. The elastic (Young's) modulus of Au and polyimide are 75 and 2 GPa, respectively, while the Poisson ratio for both materials is 0.4.

Most calculations to be reported here are for a length of $L_p=5$ μm, which is the length of the straight part of the Au leads in Fig. 1(a). We will also consider a few larger values of L_p to study the influence of the kinked ends of the leads. The distribution of displacements in the x_1 direction is shown in Fig. 4(a). The substrate displacement boundary conditions are prescribed with a value $6tu_2/L^2=0.02$ for the coefficient in Eq. (4). From Fig. 4, it is observed that the displacements in the polyimide layer are practically uniform in the x_3 direction. However, they change quite strongly with x_2, the distance from the interface. While the displacements increase

linearly with x_1 along the interface, they vary faster than linearly near the tip of the junction. Furthermore, the Au film moves almost rigidly. For this geometry, the calculation yields a tip displacement $\Delta d/2=0.056$ μm instead of the expected $\Delta U/2=0.024$ μm according to Eq. (5). In fact, the tip displacement is equal to the substrate displacement at $x_1=2.8$ μm instead of at $x_1=U/2=1.2$ μm, as assumed in Eq. (1). Thus, for this geometry, there is a multiplication factor $\zeta=2.3$ relative to Eq. (1).

A number of possible reasons for this effect come to mind, one of which is the contrast between the elastic stiffness of the Au film and the polyimide film. In fact, this turns out to be a relatively small effect as quantified below. On the other hand, Figs. 4(b) and 4(c), showing the results for $L_p=7.5$ and 10 μm, reveal that the tip displacement is quite sensitive to the length L_p of the junction. The tip displacements then are 0.076 and 0.089 μm, respectively, corresponding to $\zeta=3.17$ and 3.7. Comparison of the contours shows that the transfer of deformation from substrate to Au film is strongly affected by the free edges near the tip of the junction, at $0<x_1<U/2$, and at the end, $x_1=L_p$.

To investigate this further, we explore junctions of $L_p=5$ μm but with different etch depths $t_{etch}=0.25$ and 0.75 μm, compared to the previous value of 0.5 μm; see Fig. 5. In this figure, the case $t_{etch}=0.5$ μm has been ana-
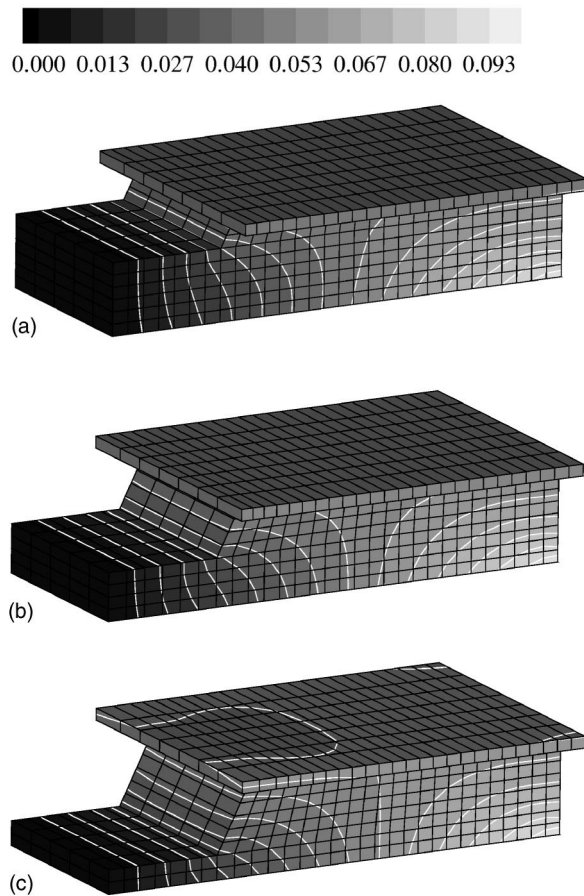
FIG. 5. Contours of equal displacement in x_1 direction (in μm) for break junctions of length $L_p=5$ μm with etch depths $t_{etch}=0.25$ (a), 0.5 (b) and 0.75 μm (c). The case with $t_{etch}=0.5$ μm is the same as that in Fig. 4(a) but is shown with different contour levels.

FIG. 6. Computed correction factor ζ relative to the Van Ruitenbeek estimate (1) in dependence of the etch depth t_{etch} (squares, at fixed length $L_p=5$ μm) and in dependence on the junction length L_p (triangles, at fixed etch depth $t_{etch}=0.5$ μm).

lyzed with a finer finite element mesh, which gives the same value of the tip displacement to all digits shown, thus proving mesh convergence. For the larger depth, Fig. 5(c), the tip displacement has increased by a factor $\zeta=0.059/0.024=2.46$, while for the two times smaller depth than previously, $\zeta=2.04$, Fig. 5(a). For an etch depth of just 0.05 μm, the tip displacement is still 1.84 times higher than the value 0.024 μm according to Eq. (5).

The various values of the correction factor ζ on Eq. (1) from these calculations are gathered in Fig. 6.

It should be noted that the displacement solution of the problem in Fig. 2 only depends on the Poisson ratios of Au and polyimide (which we have taken to be the same) and on the ratio of their Young's moduli. We have found that the correction factor ζ decreases somewhat with decreasing E_{Au}/E_p. The maximum difference from the results presented for $L_p=5$ μm occurs when $E_{Au}/E_p=1$ instead of $E_{Au}/E_p=37.5$: $\zeta=1.9$ instead of $\zeta=2.3$. The reason for this is that a relatively stiff Au layer promotes the transmission of the large displacements for x near L_p toward the Au tip at $x=U/2$. Since ζ drops by only 16% over a reduction of E_{Au}/E_p by a factor of 37.5, variations of a few percent in actual material properties have no significant effect on ζ. On
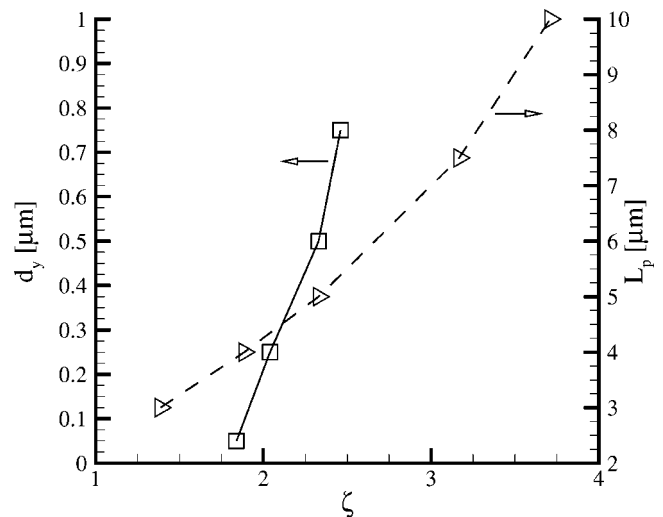
the other hand, the result does suggest that the correction can be made smaller by material selection that minimizes the modulus ratio.

The model analyzed here accounts in detail for the geometry of the bridge but not for the kink in the Au leads toward the bonding wires shown in Fig. 1(a). Instead, the length L_p is intended to include the second part in an *effective* manner. The total length of the leads in the experiments is within the range of L_p considered in Fig. 6. We do not expect that the kink itself will significantly affect the results.

IV. EXPERIMENTS

For our calibration measurements, we primarily use a setup containing a Keithley 230 voltage source and a Keithley 6517A current meter (electrometer). Furthermore, a double RC filter (two sets of $R=10$ kΩ and $C=33$ μF) as well as a tunable series resistance (to avoid high currents when the MCBJ is closed) are connected. In some cases, however, our measurements were current driven. For this, we made use of a home-made current source and voltage amplifier (a so-called Delft box). To prevent high voltage outputs, a 100 MΩ shunt resistance was connected in this case. While monitoring the junction's conductance, we slowly bend the sample until the wire suddenly breaks and the tunnel resistance jumps to an unmeasurably high value (i.e., >100 GΩ). At this point the two ends of the broken wire are rather far apart ($d>4$ nm) and we start bringing them together again by slowly pulling the rod down. As soon as a finite current is observed, we begin our calibration measurements.[13] For this, we probe the zero-bias tunnel resistance R_0 versus the pulling rod position x_2. The latter controls the interelectrode spacing d via r. All these $R_0(x_2)$ measurements are done at low bias, $V<0.2$ V, to stay within the linear regime of the tunneling IV curves (see Fig. 7 below). The break junctions are manipulated in the ambient at room temperature. We
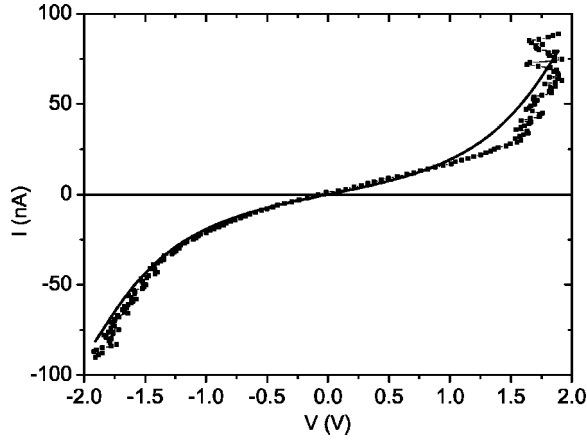
FIG. 7. Current versus voltage as measured for an open break junction with a zero-bias resistance of 60 MΩ. Note that this experiment was current driven using the Delft box setup.

adopt this calibration procedure as it is exactly the same as the one used to prepare the sample for molecular insertion.[9] Nevertheless, this implies that the calibration method introduced by Kolesnychenko *et al.*, based on Gundlach oscillations at high bias, could not be used.[14] To have an additional way to determine tunneling parameters, we choose to record current-voltage characteristics at constant d as well.

For simple tunneling between two identical metals, an exponential dependence of the zero-bias tunnel resistance R_0 on interelectrode distance d is expected:

$$R_0 \propto \exp(2\kappa d) \qquad (6)$$

where $\kappa = \sqrt{2m\phi}/\hbar$, with m the electron mass, and ϕ the size of the energy barrier. In principle ϕ is determined by the work function W of the metals involved. For gold contacts this implies $\phi = W_{\mathrm{Au}} = 5.3$ eV.[15] However, the energy barrier is significantly altered by the presence of gases and adsorbates. For example, the effective interelectrode barrier can be as high as twice the work function when He is present on the electrode surfaces.[16] For measurements in air, a practical value for the effective barrier between two gold electrodes is $\phi \approx 1$ eV.[7,17] To determine the effective barrier height ϕ independently, we measure *IV* characteristics of open break junctions. Figure 7 shows a typical result. At low bias ($|V| < 0.5$ V) we observe Ohmic behavior defining R_0. At higher voltages, the curve becomes highly nonlinear. Simmons derived the following formula for tunneling at voltages $|V| < \phi/e$:[18]

$$I = eA/4\pi^2\hbar d^2\{(\phi - eV/2)\exp[-2d/\hbar\sqrt{2m(\phi - eV/2)}]$$
$$- (\phi + eV/2)\exp[-2d/\hbar\sqrt{2m(\phi + eV/2)}]\} \qquad (7)$$

where $e = +1.6 \times 10^{-19}$ C is the electron charge and A denotes the effective surface area of tunneling. We use Eq. (7) to fit the *IV* curve in Fig. 7 (solid line). A good match is obtained for all three parameters, giving $A = 0.6 \pm 0.1$ nm^2, $d = 0.69 \pm 0.02$ nm, and $\phi = 1.1 \pm 0.2$ eV. We note that the value for A indicates that tunneling effectively takes place through a few atoms.[19] Furthermore, the value for ϕ is in accordance with literature.[7,17] Using $\phi = 1.1 \pm 0.2$ eV we ex-
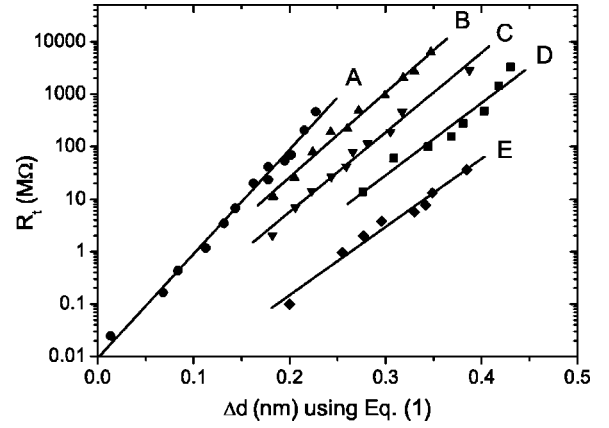

FIG. 8. Semilogarithmic plot of MCBJ zero-bias tunnel resistance R_t versus distance $\Delta d \equiv \Delta U$. The latter is calculated from the pushing rod position u_2 using Eq. (1), i.e., assuming $\zeta = 1$. Note that to the data sets, labeled A through E, an offset in the horizontal direction has been added for clarity. All curves are fitted using Eq. (6) (see Table I).

pect a coefficient $\kappa_{\mathrm{ref}} = 5.4 \pm 1.0$ nm^{-1} in Eq. (6).

Next we turn to our low-bias calibration experiments. In Fig. 8, we plot the zero-bias tunnel resistance R_0 versus the relative interelectrode displacement Δd. The latter is determined directly from the pushing rod movement u_2 and Eq. (1), i.e., $\Delta d \equiv \Delta U = 6tU/L^2 \times u_2$. Hence, no correction factor is included yet, i.e., we assume $\zeta = 1$. Figure 8 is a semilogarithmic plot showing five data sets, labeled A through E.[20] For clarity, we add an increasing offset (in u_2) to the different curves. All data sets exhibit the expected exponential relationship between tunnel resistance and interelectrode spacing. From the slope $\Delta \log_{10} R_0 / \Delta d$ we determine the values of κ as listed in Table I. On average, we have $\langle \kappa \rangle = 18$ nm^{-1}. Table I also shows the corresponding values for ϕ, giving an average value $\langle \phi \rangle = 12.5$ eV.

Inspecting Table I, we note the following. First and foremost, the values for κ are much larger than the expected $\kappa_{\mathrm{ref}} = 5.4$ nm^{-1}. Second, there is a 25% variation in the values of κ (with respect to $\langle \kappa \rangle$), translating into a variation of 50% in ϕ. It is indeed known that break junction calibration measurements often show a large variety in values of ϕ. Most likely, this is due to sample-specific differences in geometry. For example, if the nanobridge is not placed in the exact middle of the substrate and/or if the pushing rod and the bridge are misaligned, one expects a deviation from Eq. (1).

TABLE I. Experimental values for κ and ϕ as derived from Fig. 8. We obtain ζ from $\zeta \equiv \kappa/\kappa_{\mathrm{ref}}$ where $\kappa_{\mathrm{ref}} = \sqrt{2m\phi}/\hbar = 5.4$ nm^{-1}, using $\phi = 1.1$ eV.

Data set	κ (nm^{-1})	ϕ (eV)	$\zeta \equiv \kappa/\kappa_{\mathrm{ref}}$
A	22.9 ± 0.7	20 ± 1	4.3 ± 0.2
B	18.5 ± 0.7	13 ± 1	3.4 ± 0.2
C	17.5 ± 0.7	12 ± 1	3.2 ± 0.2
D	16 ± 2	10 ± 2	2.9 ± 0.3
E	15 ± 1	9 ± 1	2.8 ± 0.2

We have calculated this effect and find it to be significant, though maximally around 20% for large but possible values of misalignment.

Next we turn to the fact that our values for κ are systematically larger than expected. The average deviation is so great that it cannot be accounted for by misalignments alone. In fact, we relate the large κ values to the inhomogeneity of the MCBJ layer stack, as described above. In Table I, we determine experimental values for $\zeta = \kappa/\kappa_{\mathrm{ref}}$. This quantity varies between 2.8 and 4.3, with an average of $\langle\zeta\rangle = 3.3$. The experimental numbers are very similar to the calculated correction factors in Fig. 6. Indeed, in Fig. 6, a value $\zeta = 3.3$ corresponds to an effective bridge length $L_p = 8.2$ μm (assuming $t_p = 0.5$ μm). This is a reasonable length as can be seen from Fig. 1(a), where the distance from the kink to the center equals 6 μm. Furthermore, it justifies our assumption that the kink in the lead merely translates into an increase of the effective lead length L_p. We believe that the sample-to-sample variation in ζ values is to be attributed to both a variation in the geometric alignment and the t_{etch} dependence (see Fig. 6). Unfortunately, we were not able to separate these two effects.

Finally, to illustrate the deviation from Eq. (1), we turn to Fig. 7 again. Here we find a zero-bias resistance $R_0 = 60$ MΩ. Upon inspecting Fig. 8, we see that a resistance of 60 MΩ implies an approximate interelectrode distance $d \approx 0.23$ nm. However, the Simmons fit over the full voltage range IV curve in Fig. 7 yields $d = 0.69$ nm, which is a factor of 3 larger.

In summary, we have demonstrated that the presence of a soft (polyimide) layer changes the bending mechanics of a break junction. As a result, the calibration factor r needs to be corrected by a significant multiplication factor ζ. For our geometry, we typically find $1.8 < \zeta < 4$ for reasonable sample geometries. We compare these calculations to calibration experiments on lithographically defined break junctions and find acceptable correspondence. Knowledge of the correction factor ζ will prove useful in accurate insertion experiments for single-molecular electronics.

[1] J. Moreland and J. W. Etkin, J. Appl. Phys. **58**, 3888 (1985).

[2] C. J. Muller, J. M. Van Ruitenbeek, and L. J. de Jong, Phys. Rev. Lett. **69**, 140 (1992).

[3] J. M. Van Ruitenbeek, A. Alvarez, I. Piñeyro, C. Grahmann, P. Joyez, M. H. Devoret, D. Esteve, and C. Urbina, Rev. Sci. Instrum. **67**, 108 (1996).

[4] N. Agrait, A. L. Yeyati, and J. M. Van Ruitenbeek, Phys. Rep. **377**, 81 (2003).

[5] M. A. Reed, C. Zhou, C. J. Muller, T. P. Burgin, and J. M. Tour, Science **278**, 252 (1997).

[6] R. H. M. Smit, Y. Noat, C. Untiedt, N. D. Lang, M. C. van Hemert, and J. M. van Ruitenbeek, Nature (London) **419**, 906 (2002).

[7] C. Kergueris, J.-P. Bourgoin, S. Palacin, D. Esteve, and C. Urbina, Phys. Rev. B **59**, 12505 (1999).

[8] J. Reichert, R. Ochs, D. Beckmann, H. B. Weber, M. Mayor, and H. von Löhneysen, Phys. Rev. Lett. **88**, 176804 (2002).

[9] D. Dulic, S. J. van der Molen, T. Kudernac, H. T. Jonkman, J. J. D. de Jong, T. N. Bowden, J. van Esch, B. L. Feringa, and B. J. van Wees, Phys. Rev. Lett. **91**, 207402 (2003).

[10] J. M. Tour, L. Jones II, D. L. Pearson, J. J. S. Lamba, T. P. Burgin, G. M. Whitesides, D. L. Allara, A. N. Parikh, and S. V. Atre, J. Am. Chem. Soc. **117**, 9529 (1995).

[11] J. M. Gere and S. P. Timoshenko, *Mechanics of Materials*, 4th ed. (Stanley Thornes Publishers, Cheltenham, 1999).

[12] The x_i directions in Fig. 3 and this section are the same as in the previous section, but the origin of the x_2 axis has been moved over a distance $t/2$ to the top of the strip.

[13] We note that, due to electrode deformation, one need not obtain contact at the exact same place the junction broke.

[14] O. Y. Kolesnychenko, O. I. Shklyarevskii, and H. van Kempen, Rev. Sci. Instrum. **70**, 1442 (1999).

[15] The exact value of W_{Au} depends somewhat on the surface lattice structure: $W_{\mathrm{Au}} = 5.31$ eV for (111); $W_{\mathrm{Au}} = 5.47$ eV for (100) surfaces. For a break junction, for which it is unknown what the exact surfaces look like, this implies a natural variation in W_{Au} of order 0.1 eV.

[16] O. Y. Kolesnychenko, O. I. Shklyarevskii, and H. van Kempen, Phys. Rev. Lett. **83**, 2242 (1999).

[17] C. Lebreton, Ph.D. thesis, Université Paris 6, 1996.

[18] J. G. Simmons, J. Appl. Phys. **34**, 1793 (1963).

[19] To investigate the sharpness of our electrodes, we also measured the conductance just before the wire breaks. This results in clear plateaus at values close to integer numbers of $G_0 = 2e^2/h$ see Ref. 4 and B. J. van Wees, H. van Houten, C. W. J. Beenakker, J. G. Williamson, L. P. Kouwenhoven, D. van der Marel, and C. T. Foxon, Phys. Rev. Lett. **60**, 848 (1988). Nevertheless, and in accordance with literature, there is some variation in the exact plateau values.

[20] In one case, we found a deviating data set, giving $\kappa = 7$ nm^{-1}. In this experiment, however, we could not open the junction to resistances exceeding 100 MΩ, indicating that substantial plastic deformation had spoiled the calibration. Most likely, the polyimide was unable to accommodate the deformation and broke.